Valence-Band Electronic Structure of ZnO and ZnO:N: Experimental and Theoretical Evidence of Defect Complexes

E. Guziewicz,[1,*] O. Volnianska,[1] I.N. Demchenko,[2,3] P. Zeller,[4] M. Amati,[4] and L. Gregoratti[4]

[1] *Institute of Physics, Polish Academy of Sciences, Al. Lotnikow 32/46, Warsaw 02-668, Poland*
[2] *Institute of Plasma Physics and Laser Microfusion, 23 Hery Street, Warsaw 01-497, Poland*
[3] *Department of Chemistry, University of Warsaw, Pasteura str. 1, Warsaw 02-093, Poland*
[4] *Elettra - Sincrotrone Trieste S.C.p.A., SS 14-km Basovizza, Trieste, Italy*

(Received 22 December 2021; revised 21 June 2022; accepted 6 September 2022; published 10 October 2022)

Undoped and N-doped ZnO films are grown by atomic layer deposition under O-rich conditions. Scanning photoelectron microscopy studies carried out on the films cross sections with a state-of-the-art resolution of 130 nm, allowed the study of the electronic structure of individual crystallites. In has been found that crystallites can be divided into two types, that differ in the electronic structure of the valence band. This finding, together with the cathodoluminescence images showing clustering the acceptor- and donor-related emission, unveiled that acceptors and donors are grouped in separate regions of the ZnO and ZnO:N films. Density-functional-theory (DFT) calculations reveal that the complexes involving zinc vacancy, hydrogen, and nitrogen (in the case of ZnO:N) modify the density of states in the valence-band region, so the experimentally observed differences in photoelectron spectra between crystallites evidence the grouping of acceptor complexes in some crystallites. DFT calculations also suggest that shallow acceptor states might be of $n \cdot V_{Zn}$ origin. Nitrogen willingly joins such complexes and facilitates their formation. The separation of donors and acceptors and its tendency to group along the growth columns is of great relevance for future applications, as it indicates that eventual electronic devices should rather be constructed in a vertical architecture.

DOI: 10.1103/PhysRevApplied.18.044021

I. INTRODUCTION

Zinc oxide has been found to be inherently an *n*-type material with an electrical conductivity that can range from resistive to highly conductive and strongly varies depending on the growth method used. As charge native point defects were shown to be either deep or of high formation energy [1,2], high electron concentrations have been attributed to interstitial hydrogen impurity [3] and defect clusters or pairs present inside the material [4–7]. The presence of defect clusters has been confirmed by Raman [8,9] and Fourier-transform infrared (FTIR) spectroscopy [10] as well as by positron annihilation spectroscopy [7,11,12]. According to the present knowledge, native defect complexes, often containing hydrogen, such as V_{Zn}, nV_O ($n = 2, 3$), V_{Zn}-nH, Zn_iV_OH and others determine ZnO conductivity as they introduce shallow and deep donor and acceptor levels [13–15]. Since the O-rich or Zn-rich growth conditions determine the formation energy of native point defects [16], they also affect the formation of corresponding complexes, and thus the electrical conductivity of ZnO [11,17,18]. Additionally, it has been reported that dislocation density and strain affect electrical transport in this material as well, especially in the case of thin ZnO films [18]. The theoretical investigations indicate that doping with nitrogen gives relatively better perspective for a stable *p*-ZnO than other dopants [19]. Although the defect level of N substituting O (N_O) in ZnO was found to be as high as 1.3 eV [20], so too deep to allow for hole conductivity at room temperature, acceptor doping with nitrogen has been reported for ZnO grown using different techniques [21–30]. Theoretical studies conducted in recent years, trying to resolve this contradiction, have shown that shallow acceptor states might have more complicated physical origin than N_O, because nitrogen, like other V-group dopants [31], can form permanent complexes with V_{Zn} and/or with hydrogen, which provide shallow and deep acceptor states [2,15,32–38]. Indeed, the above complexes were detected by different experimental techniques including positron annihilation spectroscopy [39,40], Raman spectroscopy [28,38,41–44], electron paramagnetic resonance (EPR) spectroscopy [45], and these results were supported by x-ray photoelectron spectroscopy [28,38,44] and luminescence data [28,38,41,43]. Such complexes as $V_{Zn}N_O$ [33], $V_{Zn}N_OH$ [35], or the $-NH_x$ group [46], can be formed in ZnO in many different ways. Theoretical

*Corresponding author. guzel@ifpan.edu.pl

calculations have indicated that the $V_{Zn}N_O$ complex might be created by transforming the N_{Zn}-V_O complex located on the Zn-terminated surface [33], which turns out to be metastable and can evolve to the $V_{Zn}N_O$ acceptor complex with an energy lower by 0.5 eV [33]. Reynolds *et al.* [34] achieved significant hole concentration by following the above prescription experimentally. An alternative mechanism of the $V_{Zn}N_O$ complex formation, by diffusing the V_{Zn} defect towards N_O and then trapping H, was proposed by Yong *et al.* based on first-principles calculations [37]. The shallow acceptor states derived from the $(NH_4)_{Zn}$ complex were found to be thermodynamically stable under O-rich conditions, as predicted by Bang [36].

This brief summary shows that not only the efficient introduction of acceptor dopant, but also oxygen- or zinc-rich growth conditions as well as the presence of hydrogen are responsible for the formation of acceptor levels and conductivity conversion. Additionally, recent cathodoluminescence investigations have shown that the macroscopically measured p-type conductivity of ZnO may have a complicated microscopic origin, since the luminescence associated with donors and acceptors in polycrystalline ZnO films grown under O-rich conditions was found to be spatially separated and comes from different crystallites [47,48]. These results strongly suggest that ZnO layers may consist of separate domains, containing donors or acceptors, the spatial distribution of which is closely related to the microstructure of the film, i.e., the columns of growth.

First indications of separated p- and n-type regions were found on the surface of ZnO films doped with nitrogen [49] and co-doped with nitrogen and arsenic [50] in surface photovoltage measurements, but those results were obtained on the surface of the films, while present investigations were performed on the films' cross sections. The existence of n- and p-type regions was also deduced from the resistivity-distribution profiles of N-doped ZnO samples, for which the signs of the Hall-voltage signals did not change with magnetic field direction [51]. Interestingly, the surface resistivity profile confirmed the dimension of the islands with 50–100-μm scale.

The above findings motivated the scanning photoelectron microscopy (SPEM) experiment presented here, which was designed to find possible differences in the electronic structure between the columns in order to verify the thesis about the p- and n-type domains inside ZnO:N. In the performed experiment two shapes of the valence band (VB) are observed depending on the measurement site, i.e., depending on which growth column is sampled.

Correct explanation of the experimental photoelectron spectra requires a correct description of the electronic band structure of defects in ZnO. The previous theoretical studies revealed that the results strongly depend upon the exchange-correlation functional used [20,33,35,37,52–57]. A well-known deficiency of local density approximation (LDA) or generalized gradient approximation (GGA) to density functional theory (DFT) is the underestimation of a forbidden energy gap (E_g) of semiconductors due to the sublinear dependence of the total energy on the number of electrons in the system [58]. As a result, using these approaches, the energies of defect acceptor states with respect to the valence-band maximum (VBM) are calculated lower. Moreover, the LDA or GGA method leads to the increasing of delocalization of p defect states near the VBM [59]. The two approaches leading to correct E_g are the semiempirical hybrid functional (HF) method, and the LDA $+ U_d + U_p$ or GGA $+ U_d + U_p$ method in which Hubbard-like $+U$ terms [59,60] are applied to both the d (cation) and p (anion) states [54,57,61]. In particular, the significance of the $+U$ terms is additionally evident by the fact that within the last approach, both V_{Zn} or N_O are deep acceptor centers in agreement with experimental observations, which is not obtained within LDA or GGA [20,54,62].

According to this, in the first part of the paper we present the SPEM results that indicate two types of domains in ZnO:N thin film, which are reflected in different electronic structure of the VB. Next, using the GGA $+ U_d + U_p$ approach we compute the electronic structures of a number of defects and complexes involving zinc vacancy (V_{Zn}), nitrogen, and hydrogen. We find that shallow acceptor states might be of the $V_{Zn}N_O$ pair or the $V_{Zn}N_OH_i$-N_O four-constituent complex origin. We show that observed differences in the shape of the valence band can be understood in terms of grouping of donors and acceptors in separate crystallites.

II. METHODS

A. Experimental methods

For the experiment, about 2-μm-thick ZnO and ZnO:N films are grown by atomic layer deposition (ALD) on a highly resistive Si(100) substrate ($> 10^4$ Ω-cm) using diethylzinc (DEZn) and deionized water (DI) as precursors. Nitrogen is doped using ammonia water, alternatively with DI, as the oxygen-nitrogen precursor. The details of the deposition process can be found elsewhere [26,48]. Essential features of the growth procedure applied here are the low deposition temperature of 100 °C, assuring O-rich conditions in the ALD process [63] and thus facilitating creation of zinc vacancies [16], and the precursor feeding sequence in which ammonia water is alternated with deionized water in every fourth ALD cycle, which results in incorporation of the –NH group at an oxygen site in the ZnO wurtzite lattice [48]. It should be noted that the location of the –NH group (at O or Zn site) incorporated during the ALD process with the NH_4OH precursor depends on the applied precursors' feeding sequence applied in the growth procedure [28,38,64,65]. Nitrogen concentration of 1×10^{19} at./cm^3 is found from secondary

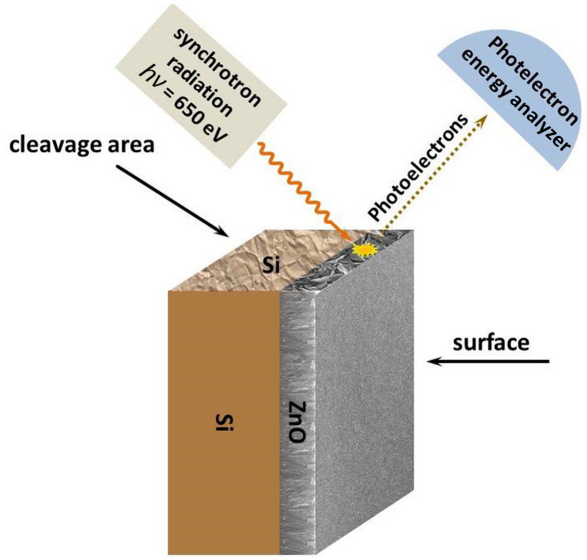

FIG. 1. Experimental scheme used in the SPEM measurements.

ion mass spectroscopy (SIMS). The samples are subjected to 4 min rapid thermal processing (RTP) in nitrogen atmosphere at 400 °C using an AccuTherm AW610 system from Alwin21 Inc. The x-ray diffractograms reveal the wurtzite-type crystal structure and show the polycrystalline nature of the ZnO and ZnO:N films with dominating [100], [002], and [110] crystallographic directions (Fig. S1 within the Supplemental Material [72]). Transmission electron microscopy (TEM) images reveal the columnar structure with ordered rows of atoms inside the grains. Details of the films structure can be found in Ref. [48].

The SPEM experiment is performed at the ESCA Microscopy beamline (Elettra, Italy) with photon energy of 650 eV and an energy resolution of 300 meV [66,67]. The spatial resolution of 130 nm, which is the *state of the art* in SPEM experiments, allowed the electronic structure to be probed inside a single column of growth. Samples are cleaved under ultrahigh vacuum (UHV) conditions to reveal an atomically clean cross-section area for a photoemission experiment. The experimental scheme is shown in Fig. 1.

B. Computational methods

The GGA calculations [68] are performed using the $+U$ corrections [60] implemented in the QUANTUM-ESPRESSO code [69]. The $+U$ corrections are imposed on d(Zn), p(O), and p(N) orbitals. Ultrasoft atomic pseudopotentials are employed [70]. The plane-wave basis with the kinetic energy cutoff of 40 Ry, which provides a good description of II-VI oxides, is applied here. The Brillouin zone summations are performed using the Monkhorst-Pack scheme with the Γ point and $2 \times 2 \times 2$ k-point mesh [71]. The 128- and 288-atom supercells are used with optimized atomic positions until the forces acting on ions are smaller than 0.02 eV/Å. More technical details about the calculation are given within the Supplemental Material [72].

We calculate the defect formation energy of defects E_{form} as [73,74]

$$E_{\text{form}} = E_{\text{tot}}(\text{host+defect}) - E_{\text{tot}}(\text{host}) + \sum n_i \mu_i + q(\varepsilon_F + \varepsilon_{\text{VBM}}) + E_{\text{correct}}. \quad (1)$$

The first two terms on the right-hand side is the total energy of the supercell with and without the defect (or complex), respectively, n_i is a number with the $+(-)$ sign corresponding to the removal (addition) of atoms, μ_i is the variable chemical potential of atoms in the solid, q is the charge state of defect (or complex), ε_F is the Fermi energy referenced to VBM, ε_{VBM} is the energy of the VBM of pure ZnO, and E_{correct} is the finite-size supercell correction [74]. The energy of ε_{VBM} is determined in line with the algorithm in Ref. [74] from the total energy difference between the pure ZnO with and without a hole at the VBM in the dilute limit. In Eq. (1) μ_i are different from the chemical potentials μ_i (bulk) of the ground state of elements (Zn bulk, O_2, H_2, and N_2). μ_i(bulk) in the standard phase are given by total energies per atom of the elemental solids: $\mu_i(\text{Zn bulk}) = E_{\text{tot}}(\text{Zn bulk})$, while $\mu_i(\text{O bulk}) = E_{\text{tot}}(O_2)/2$, $\mu_i(\text{N bulk}) = E_{\text{tot}}(N_2)/2$, and $\mu_i(\text{H bulk}) = E_{\text{tot}}(H_2)/2$. In line with our experiments, only the O-rich conditions are considered. The chemical potentials of N and H can couple with the O chemical potential. It is also considered that no additional nitrogen is introduced with oxygen during the ALD process, thus the N-poor conditions are taken into account. Thus, $\mu(\text{Zn}) = E_{\text{tot}}(\text{Zn bulk}) + \Delta H_f(\text{ZnO})$, $\mu(\text{O}) = E_{\text{tot}}(O_2)/2$, $\mu(\text{N}) = E_{\text{tot}}(N_2)/2$, and $\mu(\text{H}) = E_{\text{tot}}(H_2)/2 + 1/2\ \Delta H_f(H_2O)$. Here ΔH_f is the enthalpy of formation per formula unit, which is negative for stable compounds. ΔH_f at $T = 0$ K is obtained by considering the reaction of formation or decomposition of a crystalline from its components. Calculated ΔH_f are −3.7 (−3.6), and −2.98 (−2.96) eV for ZnO and H_2O, respectively (the experimental values are given in brackets from Ref. [75]).

The last term, E_{correct}, includes the potential alignment correction of the VBM and the image charge correction [74].

Next, we calculate the charge transition level $\varepsilon(q_1/q_2)$ between the q_1 and q_2 charge defect states that is defined as the ε_F at which formation energy of the q_1 and q_2 defect are equal [74]:

$$\varepsilon(q_1/q_2) = \frac{E_{\text{form}}(q_1; \varepsilon_F = 0) - E_{\text{form}}(q_2; \varepsilon_F = 0)}{q_2 - q_1}. \quad (2)$$

Here E_{form} is calculated according to Eq. (1). We note, that $\varepsilon(q_1/q_2)$ are independent of the growth conditions and can

be observed in cathodoluminescence measurements, where a defect in the stable charge state fully relaxes to its ground structure after the transition.

A few technical aspects of the calculations require a comments. Before starting the self-consistent field calculations, slightly asymmetric structures around the defects are introduced. Thanks to such a symmetry breaking, all possible hole configurations in terms of their positions and spins are considered and, as a result, the energetically lowest solution is chosen (see Sec. S5 within the Supplemental Material [72]).

The gain in the formation energy of the complexes is evaluated as the difference in the formation energy between isolated constituents of the complex and the complex itself for a given Fermi level:

$$E_{\text{gain}} = \sum E_{\text{form}}(\text{constituent}) - E_{\text{form}}(\text{complex}). \quad (3)$$

The positive gain energy values indicate an energetic preference for the defect complex to be formed. In this work for three-constituent complexes, E_{gain} can be represented as a gain energy with respect to the three individual defects or the E_{gain} of one point defect attached to a defect pair. For four-constituent complexes E_{gain} is formation energy gain of one point defect attached to the triangles.

III. RESULTS

A. Experimental results

Each measurement is started in "imaging" mode [66] in order to visualize the appearance of the obtained cross-section area. Although the cross section turned out to be rather rough, as seen in Fig. 2(a) (ZnO) and Fig. 2(b) (ZnO:N), it resembled that obtained in SEM microscopy (see Ref. [47]), and the columns of growth are easily distinguished. In the next step, in the "spectroscopy" mode, the PES spectra of the Zn2p, Zn3d, O1s and C1s core levels and the valence band (VB) are measured at selected points, as shown in Figs. 2(a) and 2(d) (red letters). The N1s signal is found to be below the detection limit as a result of both a low doping concentration and a small sampling area. XPS survey spectra showed only peaks coming from zinc oxide, while carbon contamination is very low at the measured points.

It is found that the FWHM value of the Zn3d level is the same (1.67 eV) for all the measured columns from the cross section of ZnO [Fig. 2(b)] and ZnO:N [Fig. 2(e)] films. In the case of ZnO, the energy position of the *Zn3d* is the same within the experimental resolution [Fig. 2(b)], while a 400-meV shift of this peak is observed for ZnO:N between different grains [Fig. 2(e)]. Such a shift can be understood in terms of a change in the Madelung energy and is related to the change of the Fermi level position

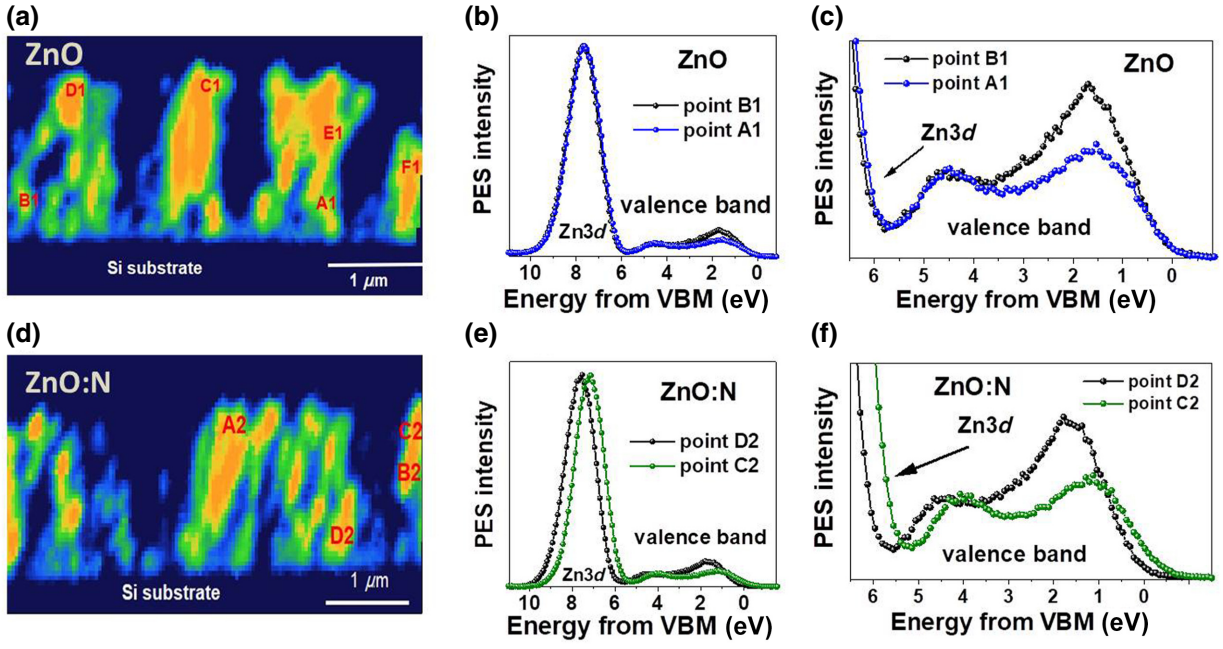

FIG. 2. SPEM images of the films' cross sections measured from the Zn3d for (a) annealed ZnO and (d) ZnO:N films. The colors are chosen to emphasize the details of the cleavage morphology, with orange being high and blue being low signal intensity. (b),(e) PES spectra of ZnO (b) and ZnO:N (e) in the valence band and Zn3d region; (c),(f) PES spectra of ZnO (c) and ZnO:N (f) in the valence-band region.

in the material [76]. As a result, the valence-band edge is located higher, which favors hybridization of the valence band with shallow acceptor levels.

However, the most substantial difference in the photoemission response is observed in the valence-band region. The valence-band spectrum of zinc oxide derives from the hybridized O2*p* and Zn4*s* orbitals and consists of two peaks, one with a maximum at about 1.75 eV and the second one at about 4.5 eV below the valence-band edge. The considerable intensity change of the former PES maximum can be easily noticed, while the intensity of the second maximum remains untouched [Figs. 2(c) and 2(f)]. It is worth noting that similar changes occur in the PES spectra of both ZnO as well as ZnO:N sample, however, in the latter case they are accompanied by the valence-band shift towards the Fermi level. In semiconductors the valence-band maximum (VBM) and binding energy (BE) of shallow core levels probe the Fermi-level position in the band gap, so the last observation suggests some acceptor states in the growth columns showing the lower "1.75-eV band" intensity. It should be stressed that although the PES spectra are measured at different points along the film cross section, only two shapes of the valence band, as presented in Figs. 2(c) and 2(f), are found for every film.

A comparison of the PES valence band spectra reveals that while the spectra with higher "1.75-eV band intensity" are the same for ZnO and ZnO:N, the PES spectra with lower "1.75-eV band intensity" are different in both films. In the case of ZnO:N films the "1.75-eV" band is even lower and shifted to lower BE, which points at a different origin of the valence-band intensity lowering.

Differences in the shape of the ZnO valence-band spectra are already reported in the literature. Such an effect has been shown for single-crystal ZnO when Zn-polar and O-polar surfaces were investigated and photoemission signal has been collected perpendicularly to the crystal surface, i.e., for a take-of angle of 90° [77–79]. In such a case, photoemission intensity from the lowest binding energy states, sometimes called *subpeak*, has been found to be significantly more intensive for the Zn-polar face compared to the O-polar face, for *m* plane is situated between them, while the intensity of the higher binding energy states is the same for all three polarities [77]. This effect was reported for a range of single ZnO crystals grown by the hydrothermal, pressurized-melt and chemical vapor transport techniques as well as for thin ZnO films obtained by pulsed laser deposition [77,78]. Moreover, it disappears for measurements performed for lower take-off angles and photon excitation energy lower than 600 eV, which rather excludes the surface-related character of the subpeak and accounts for its bulk-related origin. The latter conclusion is also supported by the measurements showing that the subpeak effect appears in the valence-band spectra regardless of the surface preparation and chemical-treatment conditions [78,79]. The band-bending origin was also excluded as a similar effect was observed for samples with carrier concentration ranging from 10^{14} till $10^{20}/\mathrm{cm}^3$, [77–79]. Based on the above considerations, the surface-related effect was excluded, however, the exact origin of this peak has not been discovered. Interestingly, the subpeak effect was also reported for photoemission spectra taken for low-dimensional ZnO structures, which do not have any Zn-polar or O-polar faces [80–83]. The spatially resolved valence-band photoemission spectra of ZnO nanorods were measured by SPEM at various positions, near the center and sidewall regions of the nanorods [80,81]. The intensity of the subpeak was found higher near the edge of the nanorod, which was tentatively interpreted as caused by the 2*p* dangling bonds of O ions, however, without any further confirmation. A similar effect was reported by Ansari *et al.* who showed the XPS valence-band spectra for pure and modified ZnO powder [82]. The latter one reveals lower intensity of the valence-band peak close to the valence-band edge, which has been attributed to the band-gap narrowing and oxygen vacancies that were indirectly observed in the shape of the 1*s*(O) core level. Schmeißer *et al.* [83] have found the lower intensity of the low binding energy part of the XPS valence-band spectrum for amorphous ZnO.

All the experimental results mentioned above indicate that the lowering of the density of states near to the valence-band edge is a bulk-related effect, which it should be rather attributed to defects, defect complexes and, maybe, structural differences in the ZnO lattice, which, in the case of single crystals, may be closely related to different surface polarity. The only DFT calculations trying to address the problem of valence-band shape modification of ZnO with native defects were performed by Wang *et al.* [84]. They assigned the valence-band differences to impurity states that appear near to the valence-band edge because of oxygen vacancies.

In the next paragraph we carefully analyze the various defects and defect complexes that may exist in ZnO and show that they can contribute to changing the shape of the valence band. We calculate the formation energy of various defect complexes that are expected to appear in ZnO:N grown by ALD under O-rich conditions and postgrowth annealed. Then, we calculate the total density of states in order to explain the differences in the shape of the valence band observed in the SPEM experiment.

B. DFT results

The application of $U_{\mathrm{Zn}} = 10$ eV, $U_{\mathrm{O}} = 7$ eV, and $U_{\mathrm{N}} = 7$ eV [54,61,88,89] terms reproduces both the experimental lattice parameters of wurtzite (*w*) ZnO ($a = 3.223$ Å and $c = 5.24$ Å), as well as the experimentally correct $E_g = 3.37$ eV and the energy of the core *d*(Zn) band, centered about 8 eV below the VBM [90,91]. It is reflected in

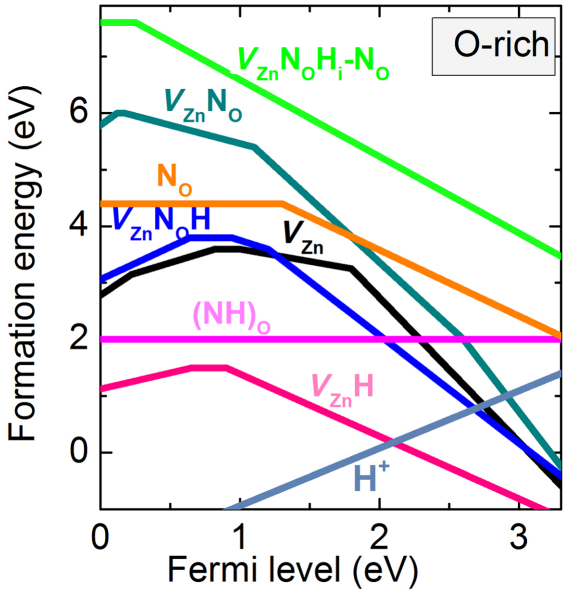

FIG. 3. Formation energies of investigated defects as a function of the Fermi energy for ZnO grown in O-rich condition.

the density of states (DOS) results shown within the Supplemental Material [72] (Fig. S5) that agree well with the measured PES spectra [Figs. 2(b) and 2(c)].

The results of calculations of defect formation energies and the thermodynamic charge transition levels are presented in Fig. 3 and Table I. In Fig. 3 the slope of each line corresponds to a stable charge state, while the points represent the $\varepsilon(q_1/q_2)$. If the calculated $\varepsilon(q_1/q_2)$ lies in the forbidden gap we perceive it as a stable state, in contrast to the transition levels that are resonant and located in the VBM or the CBM. In particular, we note that the $+/-$ level of H_i is calculated to be resonant with the conduction band, which suggests that the shallow donor level is observed, in agreement with the previous calculations [86].

In Table I, we compare the calculated $\varepsilon(q_1/q_2)$ levels with the corresponding results of other DFT studies. We note that the current GGA+U results, in particular for V_{Zn} and nitrogen impurity, agree with $\varepsilon(q_1/q_2)$ values obtained by HFs when Janh-Teller perturbation is taken into account [15,55,86]. For example, we find that formation energy of neutral V_{Zn} is 3.5 eV and four thermodynamic charge transition levels are predicted to be within the band gap, $+2/+ = 0.22, +/0 = 0.82, 0/- = 1.15$, and $-/-2 = 1.75$ eV (Fig. 3). All values are calculated with respect to the VBM and are in agreement with the values obtained in other works by HF approaches [52,55]. When V_{Zn} is formed in the wurtzite structure, it results in the four dangling Zn—O bonds. These four sp^3(O) orbitals of O neighbors combine into a singlet and a quasitriplet (t_2) that is higher in energy. The two holes at the defect states induce a Janh-Teller effect, which drives a splitting of spin-down-quasitriplet state into an occupied singlet and an empty doublet that is located at about 2.4 eV above the VBM (Fig. S6 within the Supplemental Material [72], we plot the DOS for spin-up and spin-down states of vacancy as positive and negative values), reflecting deeplike character of vacancy acceptor states. When the V_{Zn} is passivated by H^+, they form the stable complex as $V_{Zn}^- + H_i^+ \rightarrow V_{Zn}H_i$ with about 2.0 eV of the formation energy gain. In this case H_i is located at one of the four V_{Zn}^- dangling sp^3(O) bonds lowering vacancy symmetry from C_{3v} to C_2. Moreover, in undoped ZnO, the V_{Zn}-H complex

TABLE I. Calculated thermodynamic charge transition level of defects, in eV. In this work and Refs. [42,62] the GGA + U_d +U_p method is used and in all other references HF approaches were performed.

$\varepsilon(q_1/q_2)$	V_{Zn}	$V_{Zn}H$	N_O	$V_{Zn}N_O$	$V_{Zn}N_OH$	$V_{Zn}N_OH$-N_O
+2/+	0.22 here	0.2 here				
+2/+	0.23 [55], 0.25 [56], 0.83 [62]	0.2 [15], 0.22 [55], 0.87 [62]				
+/0	0.82 here	0.65 here	-	0.12 here	0.64 here	
+/0	0.81 [56], 0.89 [55], 0.85 [62]	0.65 [55], 0.7 [15], 0.89 [62]				
0/-	1.15 here	0.95 here	1.49 here	0.17 here	0.9 here	0.225 here
0/-	0.69 [52], 0.96 [62], 1.39 [55]	1.1 [62], 1.26 [55], 1.32 [15]	1.3 [20], 1.46 [85], 1.47 [86]	0.16 [33], 0.28 [35]	0.77 [35]	
0/-	1.4 [56], 1.15, 1.5 [53]		1.8 [27], 2.04 [55], 2.1 [87]	0.2 [27,37]	0.92 [42]	
-/-2	1.75 here, 1.25 [62], 1.96 [56]			1.25 here	1.2 here	
-/-2				1.2 [35]	1.15 [35], 1.5 [42]	
-2/-3				2.6 here		
-2/-3				3.3 [35]		

is the dominant deep acceptor due to relatively low E_{form} (Fig. 3) and thus, calculations suggest that acceptor states observed in Figs. 2(a)–2(c) might be of $n \cdot V_{Zn}H_i$ origin.

In agreement with the HF calculations [74,85,86], the current study has shown that nitrogen substituting for oxygen forms a deep acceptor state as 0/- is 1.49 eV (Fig. 3). The single hole at the threefold-degenerate state induces a strong Jahn-Teller distortion and a splitting quasitriplet state into occupied doublet and empty singlet, which is located about 2.5 eV above the VBM in agreement with the HF results [85,86] (Fig. S6 within the Supplemental Material [72]).

The energy level of the N_O can be affected by its local surrounding, here we investigate $V_{Zn}N_O$, $V_{Zn}N_OH$, and the $V_{Zn}N_OH_i$-N_O complexes. Equilibrium configurations of complexes are shown in Figs. 4 and Fig. S8 within the Supplemental Material [72].

V_{Zn} and N_O form the stable complex, for example, at 0.82-1.15 eV Fermi energy region as $V_{Zn} + N_O \rightarrow [V_{Zn}N_O]$ (see Fig. 3). They also can create $V_{Zn}^{+} + N_O \rightarrow [V_{Zn}N_O]^{+}$, $V_{Zn}^{-} + N_O \rightarrow [V_{Zn}N_O]^{-}$, and $V_{Zn}^{-} + N_O^{-} \rightarrow [V_{Zn}N_O]^{-2}$ complexes. For $V_{Zn}N_O$ pair its formation energy gain is predicted to be 1.9 eV, with respect to the isolated V_{Zn} and N_O (comparable value, 1.7 eV, was obtained in Ref. [35]). This implies the stability of such complexes at typical growth or annealing temperatures.

Acceptor clustering stems from the formation of quasimolecular bonds between dopants, which was suggested to be a universal phenomenon in semiconductors [92]. From this point of view, the $V_{Zn}N_O$ pair is created by the formation of quasimolecular bonds between V_{Zn} and N_O. The spin-density isosurfaces of V_{Zn}, N_O, and the $V_{Zn}N_O$ pair are shown in Fig. 5. Three holes in $V_{Zn}N_O$ states are located

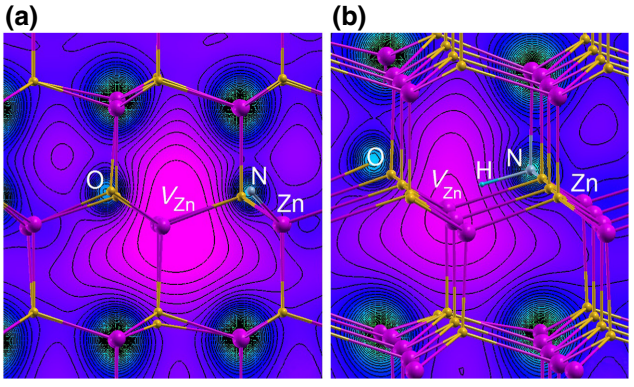

FIG. 4. Calculated atomic configurations and the electron density isolines for (a) $V_{Zn}N_O$ and (b)$V_{Zn}N_OH$. One can see the large distortion of the crystal structure by the formation of defects. The rainbow-type color coding refers to pink as regions of minimum charge density, which increases gradually as violet, blue, green, and finally to red as the region of maximum charge density. Contours go 0.0009 to 0.5 electron/Bohr^3.

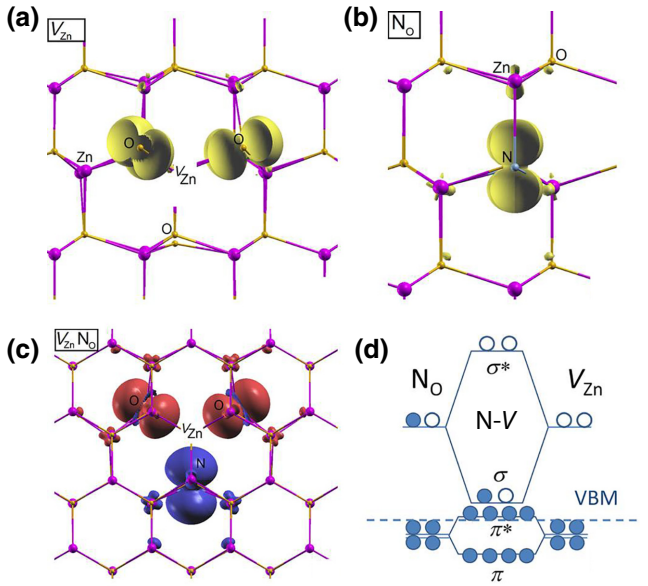

FIG. 5. (a)–(c) The isosurfaces of spin-density distributions for the empty orbitals in the defect states corresponding to 0.004 electron/Bohr^3. (a) V_{Zn}, (b) N_O, (c) $V_{Zn}N_O$ complex is shown in the (x,y) plane. Blue and red color correspond to the different spin orientations. (d) Simple scheme explains the formation of $V_{Zn}N_O$ complex by creation of molecularlike bonding-antibonding states.

on two sp^3(O) and one sp^3(N) dangling bonds, neither the shape nor the spin structure is the sum of those of two isolated defects. In particular, in the former case spin densities are more delocalized, since they comprise long-range tails engaging p orbitals of distant O ions which reflects the hybridization of the defect states with the VBM. The VBM is mostly built from p-like anion orbitals. The total spin of V_{Zn} and N_O is 1 and 1/2, respectively, while 1/2 spin is assumed in the case of the complex (see the Supplemental Material [72]). The spin-density results are supported by the density of states calculations presented in Figs. 6 and S6 within the Supplemental Material [72]. One can see that the $V_{Zn}N_O$ levels are built from p(O) and p(N) orbitals

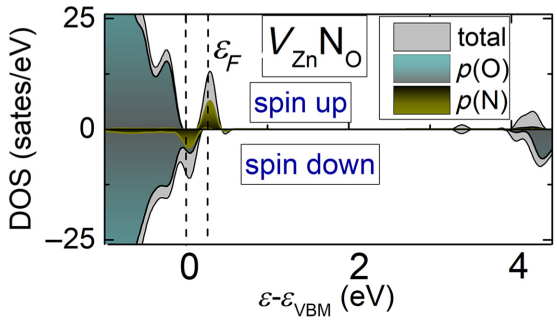

FIG. 6. Total density of states and the contributions of p(O) and p(N) orbitals $V_{Zn}N_O$ in ZnO.

and complex states are hybridized with the valence bands. According to the pseudomolecular bond model there is a formation of π and σ combinations with p-like (p_{xy} and p_z) orbitals of the V_{Zn} and N_O [Fig. 5(d)]. The bonding combinations are lower in energy than the levels of isolated defects (Fig. S6 within the Supplemental Material [72]), and in the case under study they are degenerate with the continuum of the valence band of ZnO (see Figs. 6 and S6 within the Supplemental Material [72]). The complex states including one hole degenerate with the VBM bands. The antibonding states of pairs (denoted by stars) are higher in energy. The σ splitting is stronger than the π splitting because of the stronger overlap of orbitals in the xy orientation, and thus a stronger coupling therein. Although the presented mechanism and diagram are very simplified, they can be universal and help in predicting similar complexes in semiconductors. It will be shown below that the similar scheme is realized in the case of four-constituent complexes. According to GGA+U_d+U_p calculations the $V_{Zn}N_O$ containing three holes acts as a shallow acceptor, with the level $0/- = 0.17$ eV above the VBM (Table I). Also, we find that $+/0 = 0.12$ eV, this defect level is located near the VBM and there can be the strong hybridization of the defect's p states with the VBM states that mostly are built from p(O) electrons. The $V_{Zn}N_O$ pair can be associated with the acceptor levels observed in the presented photoemission experiments.

When H passivates the $V_{Zn}N_O$ pair, it is located on the sp^3 N_O-dangling bond (Figs. 4 and Fig. S9a within the Supplemental Material [72]) due to the fact that the $(NH)_O$ complexes are much more stable than H_i [93]. H_i accommodation within the complex not only lowers the formation energy (Fig. 3), but also stabilizes the high spin state with the total spin of 1 (see the Supplemental Material [72]).

In agreement with previous reports [35,42] we obtain that an acceptor level $0/- = 0.9$ eV of the $V_{Zn}N_OH$ complex is higher than that of $V_{Zn}N_O$ (Table I). In spite of it, we note, that introduction of these complexes might provide the first step towards p-type doping before annealing. By optimizing the growth and annealing conditions, the activation of large concentrations of $V_{Zn}N_O$ acceptors may be possible. For example, E_{form} of $V_{Zn}N_OH$ complex is about 1.2 eV lower than the sum of the formation energies of the $[V_{Zn}N_O]^-$ complex and the H^+ interstitial separately. This shows that passivation by H results in a three-constituent-complex stabilization and making it easier to form. Also, it has been confirmed that the $V_{Zn}N_OH_2$ complex is also stable [37].

Moreover, we find that the shallow acceptor states might be due to larger defect clusters passivated by hydrogen, for example, four-constituent-complex $V_{Zn}N_OH_i$-N_O origin (see Table I and the Supplemental Material [72]). The acceptor level of such a complex is found to be 0.22 eV above the VBM. According to Fig. 3 $[V_{Zn}N_OH_i] + N_O \rightarrow [V_{Zn}N_OH_iN_O]$ and $[V_{Zn}N_OH_i]^- + N_O \rightarrow [V_{Zn}N_OH_iN_O]^-$ are possible charge states of the four-constituent complex. Complex forms with $E_{gain} = 0.6$ eV. Complex levels are strongly bonded with the host valence bands (Figs. S7–S9 within the Supplemental Material [72]). Three holes in the complex states are located on sp^3(O) and sp^3(N) dangling bonds, and neither the four-constituent complex spin-density distribution nor the structure is the sum of two isolated constituents (see Fig. S9 within the Supplemental Material [72]).

The comparison of the calculated DOSs with the photoelectron spectra shows a strong qualitative agreement between the theory and experimental results. The normalized DOS results of undoped and defected ZnO presented with a large spline (Fig. 7) can explain the observed differences in the valence-band spectra accompanied with the shift of states near the VBM [Fig. 2(f)]. The bonding and not fully occupied defect complex states hybridize with the VBM continuum, that is observed in SPEM experiments as a shift of the VBM. We also note that like for photoelectron spectra, DFT calculated d(Zn) core levels are not shifted for defects in undoped ZnO, but there is a shift of the d(Zn) level, of about 0.2–0.3 eV, between pristine ZnO and ZnO with nitrogen complexes. We explain this by hybridization between p(O) − p(N) − d(Zn) core states.

Finally, we summarize the efficiency of formation of complexes via the perspective of an experimental growth process. According to Fig. 3, the E_{form} of complexes are large on the scale of the formation energy of its constituents, and hence their concentrations are small [94,95]. In spite of this, when complexes occur under nonequilibrium conditions, their concentration can be significantly different from what Fig. 3 implies. For example, if the isolated constituents are formed in the first phase, the complex formation can happen via diffusion of the defects [37,96]

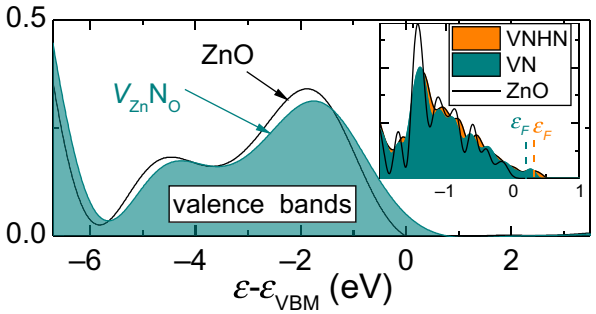

FIG. 7. The normalized total density of states of ZnO and the $V_{Zn}N_O$ in ZnO. The results are qualitatively correlated with experiment (Fig. 2), which suggests that the $V_{Zn}N_O$ is responsible for the p-type areas in the crystal. The defect $V_{Zn}N_O$ and $V_{Zn}N_OHN_O$ empty states at about 0.2 eV above VBM is seen in the inset, Fermi levels are depicted (see within the Supplemental Material [72] for details). The DOSs of complexes correspond to the sum of spin-up and -down states.

and/or strong bond between constituents (in relatively high concentrations of them). Thus, from this perspective, we suppose that E_{gain} values provide a better measure of whether the complexes do form or not. For instance, if a diffusing zinc vacancy comes across a nitrogen, they will bind together as long as there is sufficient attraction, which should be the case as there is a tendency to favor acceptor-acceptor clusters. According to Ref. [37], V_{Zn} can diffuse easily within ZnO:N under the normal growth conditions (approximately 150 °C) with the energy barrier for V_{Zn} migration around N_O about 1.1 eV. In the case of V_{Zn} diffusing around $(NH)_O$ the energy barrier is much lower [37]. We find that the formation energy gains of the $V_{\text{Zn}}N_O$H complex are 3.3, 1.7, and 1.2 eV with respect to the three individual defects, to the $(NH)_O$ and zinc vacancy separately, and to the $V_{\text{Zn}}N_O$ pair and H interstitial separately, respectively (Fig. 3). The forming of $V_{\text{Zn}}N_O$H groups that takes place with relatively low formation energies might provide the first step towards p-type doping before annealing that is performed at temperatures T_a much higher than the growth temperature. We can approximately estimate the required T_a at which the H removal from the $V_{\text{Zn}}N_OH_i$ complex starts as [97]

$$T_a = \frac{E_d}{k_B ln(\tau \nu)}, \tag{4}$$

where E_d is the thermal dissociation energy given by the sum of E_{gain} and the migration energy, E_m. k_B is the Boltzmann constant, $\nu \approx 1.6 \times 10^{13}$ s^{-1} is the frequency of atomic vibrations, τ is the characterization time for complex dissociation, here we consider it as the time of the annealing. $E_{\text{gain}} = 1.2$ eV and $E_m = 1.25$ eV [98] (the migration barrier interstitial hydrogen in N-doped ZnO), the E_d is estimated as 2.45 eV. Thus, the $V_{\text{Zn}}N_O$H complex can start to dissociate to the $V_{\text{Zn}}N_O$ and H interstitial at temperatures approximately 520 °C for $\tau \approx 240$ s that is in reasonable agreement with experimental temperatures and time of annealing (see Sec. II A). We note, that estimated E_d of the $V_{\text{Zn}}N_O$H complex to $(NH)_O$ and V_{Zn} is larger by approximately equal to 0.45 eV.

The defect formation energy of the four constituent complex is very high, approximately equal to 7.6 eV. But this complex may be created from the bonding between the previously formed $V_{\text{Zn}}N_O$H complex and N_O impurity. However, E_{form} of this complex will be lower under Zn-rich conditions. The good effectiveness of ZnO doping requires high defect concentrations, as the acceptor states are formed from the superposition of levels of various local configurations. Here, the different origin for shallow acceptor states can take place as they come from $V_{\text{Zn}}H_i$, $V_{\text{Zn}}N_O$ pairs or three-, four-constituent complexes, etc.

Generally, when the sample is p-type, the H^+ hydrogen and so called "generic" donors (e.g., oxygen vacancies, V_O) may compensate the holes generated by the acceptors. But the investigated samples are converted to p-type after annealing, and we note that hydrogen in ZnO is mobile with the low diffusion barrier of approximately 0.5–0.7 eV, so hydrogen is expected to be removed during the annealing. Indeed, we find out that after annealing at 800 °C, the H concentration is low, about 1–2 $\times 10^{18}$ cm^{-3}, and it is introduced into ZnO in the form of NH_x and, possibly, also CH_x groups. On other hand, H decorates isolated defects and promotes formation of complexes. Additionally, we consider O-rich growth conditions as they facilitate the maximum reduction of oxygen vacancies. It should be remembered that, contrary to hydrogen, the presence of such donors as V_O is detrimental for p-type doping as it leads to the occupation of the antibonding acceptor states by electrons, which gives rise to the weakening of the complex bonding [92]. It is also worth noting that, in spite of our extensive investigations on p-type conductivity performed in the last 10 years, we have never observed the macroscopic p-type conductivity in samples that are grown under Zn-rich conditions.

Finally, the creation of such complexes as $V_{\text{Zn}}N_O$ is sensitive to the local atomic structure and perturbations. The introduction of even slightly asymmetric structures around the complexes can result in large changes in their symmetry structure, the total energies and electronic and spin configurations (see the Supplemental Material [72] and Refs. [15,54]). We suggest that the energetically lowest mechanism for complexes' formation may be driven by microstrain processes or occur under the surface proximity.

IV. SUMMARY AND CONCLUSIONS

In summary, we show the first photoelectron spectra taken at the atomically clean cross section of ZnO/Si and ZnO:N/Si films cleaved under UHV conditions. The lateral SPEM imaging with a resolution of 130 nm allows investigation of the electronic structure of a single grain. Two types of micrograins are found both in ZnO and ZnO:N films based on the shape of the valence band.

DFT calculations show that $n \cdot V_{\text{Zn}}$ and $V_{\text{Zn}}N_O$ complexes, easily formed in ZnO and ZnO:N grown under O-rich conditions and further stabilized by hydrogen, provide shallow acceptor states and influence the DOS in the valence-band region in a manner similar to that observed in the SPEM experiment. Nitrogen, when doped, willingly joins such complexes and facilitates their creation. The results presented here point at a dual role of nitrogen as a dopant in ZnO, which can both passivate shallow donors and facilitate creation of $n \cdot V_{\text{Zn}}$ complexes providing shallow acceptor levels. Hydrogen lowers the formation energy of the $V_{\text{Zn}}N_O$ complex, but the appearing $V_{\text{Zn}}N_O$H complex is found to be a deep acceptor.

Taking into account the conditions of the ALD process performed and based on the DFT calculations, the scenario for achieving the p-type conductivity in the investigated

samples is as follows. The ALD process is carried out under oxygen-rich conditions, which lowers the energy of zinc vacancy formation and increases its concentration. Nitrogen is introduced into the layer as the -NH group, which is a consequence of the surface chemical double-exchange reaction between diethylzinc and ammonia water in the ALD process. As a result of zinc vacancy diffusion, the $V_{Zn}N_OH$ complex is formed, which is a deep acceptor. The annealing process is necessary to remove hydrogen from the complex. The created $V_{Zn}N_O$ complex is a shallow acceptor, so annealing activates the hole conductivity at room temperature.

Probably the most important finding of this paper is the confirmation of the acceptor and donor domains in ZnO layers, as indicated by the previous CL studies, showing the clustering of donor and acceptor luminescence in different crystallites. Two shapes of the valence band found at the ZnO and ZnO:N films cross section, based on the performed DFT calculations, can be assigned to *p*- and *n*-type domains present inside the films. DFT calculations show that the presence of $V_{Zn}N_OH$ and $V_{Zn}N_O$ complexes modifies DOS in the valence-band region, so two shapes of the valence band can be assigned to grouping of acceptors in separate domains.

The reason for donor and acceptor domains is not entirely clear and requires further research. Some indications are provided by earlier photoemission studies carried out on Zn- and O-polar surfaces of single ZnO crystals and the SPEM measurements of ZnO nanostructures, where similar modifications of the valence-band shape are recorded. Based on this, it might be supposed that the formation of acceptor complexes is associated with the distortion of the crystal lattice, so it can be assumed that microstrain plays a role here. The presented DFT calculations confirm that the creation of defect complexes is very sensitive to the local structure and atomic perturbations.

The separation of donors and acceptors is of great relevance for future applications. On the one hand, this means that it is possible to obtain a homogeneous ZnO acceptor conductivity without the accompanying donors at least on the nanometer scale. On the other hand, the connection of these areas with crystallites and growth columns indicates that eventual devices should rather be constructed in a vertical architecture so that the transport of current carriers takes place along the growth columns.

ACKNOWLEDGMENTS

The work is a result of the research Project No. 2018/31/B/ST3/03576 founded by the National Science Centre, Poland. The authors acknowledge the support from Elettra Sincrotrone Trieste (Proposal ID 20180152-Elettra). DFT calculations were performed in ICM at University of Warsaw (Grant No. G16-11).

[1] A. Janotti and C. van de Walle, Native point defects in ZnO, Phys. Rev. B **76**, 165202 (2007).

[2] R. Vidya, P. Ravindran, H. Fjellvåg, B. Svensson, E. Monakhov, M. Ganchenkova, and R. M. Nieminen, Energetics of intrinsic defects and their complexes in ZnO investigated by density functional calculations, Phys. Rev. B **83**, 045206 (2011).

[3] Y. K. Y.R. Park and J. Kim, Effect of hydrogen doping in ZnO thin films by pulsed DC magnetron sputtering, Appl. Surf. Sci **255**, 9010 (2009).

[4] K. Tang, S. Gu, S. Z. J.D. Ye, R. Zhang, and Y. Zhen, Recent Progress of the native defects and p-type doping of zinc oxide, Chin. Phys. B **26**, 047702 (2017).

[5] J. Bang, J. Kim, C. Park, F. Gao, and S. Zhang, Understanding the presence of vacancy clusters in ZnO from a kinetic perspective, Appl. Phys. Lett. **104**, 252101 (2014).

[6] D. Kim, G. Lee, and Y. Kim, Interaction of zinc interstitial with oxygen vacancy in zinc oxide: An origin of n-type doping, Sol. State Commun. **152**, 1711 (2012).

[7] Z. Wang, S. Su, M. Younas, F. Ling, W. Anwand, and A. Wagner, The Zn-vacancy related green luminescence and donor-acceptor pair emission in ZnO grown by pulsed laser deposition, RSC Adv. **5**, 12530 (2015).

[8] M. Gluba, N. Nickel, and N. Karpensky, Interstitial zinc clusters in zinc oxide, Phys. Rev. B **88**, 245201 (2015).

[9] S. Pal, N. Gogurla, A. Das, S. Singha, P. Kumar, D. K. ad A. Singha, S. Chattopadhyay, D. Jana, and A. Sarkar, Clustered cvacancies in ZnO: Chemical aspects and consequences on physical properties, J. Phys. D.: Appl. Phys. **51**, 105107 (2018).

[10] K. Senthilkumar, T. Yoshida, and Y. Fujita, Formation of D-V(Zn) defects and possible p-type conductivity of ZnO nanoparticle via hydrogen adsorption, J. Mater. Sci. **53**, 11977 (2018).

[11] Z. Wang, C. Luo, W. Anwand, A. Wagner, M. Butterling, M. A. Rahman, M. R. Phillips, C. Ton-That, M. Younas, S. Su, and F. Ling, Vacancy cluster in ZnO films grown by pulsed laser deposition, Sci. Rep. **9**, 3534 (2019).

[12] V. P. I. Makkonen, E. Korhonen, and F. Tuomisto, Identification of vacancy defect complexes in transparent semiconducting oxides ZnO, In_2O_3 and SnO_2, J. Phys.:Conf. Matter **28**, 224002 (2016).

[13] R. Schifano, R. Jakiela, K. K. A. Galeckas, K. Johansen, and L. Vines, Role of intrinsic and extrinsic defects in H implanted hydrothermally grown ZnO, J. Appl. Phys. **126**, 125707 (2019).

[14] R. Heinhold, A. Neiman, J. Kennedy, A. Markwitz, R. Reeves, and M. Allen, Hydrogen-related excitons and their excited-state transitions in ZnO, Phys. Rev. B **95**, 054120 (2017).

[15] Y. K. Frodason, K. M. Johansen, T. S. Bjørheim, B. G. Svensson, and A. Alkauskas, Zn vacancy-donor impurity complexes in ZnO, Phys. Rev. B **97**, 104109 (2018).

[16] A. Janotti and C. van de Walle, Fundamentals of zinc oxide as a semiconductor, Rep. Prog. Phys. **72**, 126501 (2009).

[17] E. Przezdziecka, E. Guziewicz, D. Jarosz, D. Snigurenko, A. Sulich, P. Sybilski, R. Jakiela, and W. Paszkowicz, Influence of oxygen-rich and zinc-rich conditions on donor and acceptor states and conductivity mechanism of

ZnO films grown by ALD-experimental studies, J. Appl. Phys. **127**, 075104 (2020).

[18] S. Mishra, E. Przezdziecka, W. Wozniak, A. A. R. Jakiela, W. Paszkowicz, A. Sulich, M. Ozga, K. Kopalko, and E. Guziewicz, Structural properties of thin ZnO films deposited by ALD under O-rich and Zn-rich growth conditions and their relationship with electrical parameters, Materials **14**, 4048 (2021).

[19] C. Park, S. Zhang, and S.-H. Wei, Origin of p-type doping difficulty in ZnO: The impurity perspective, Phys. Rev. B **66**, 073202 (2002).

[20] J. L. Lyons, A. Janotti, and C. G. V. de Walle, Why nitrogen cannot lead to p-type conductivity in ZnO, Appl. Phys. Lett. **95**, 252105 (2009).

[21] J. Bian, X. Li, C. Zhang, W. Yu, and X. Gao, p-type ZnO films by monodoping of nitrogen and ZnO-based p-n homojunctions, Appl. Phys. Lett. **85**, 4070 (2004).

[22] Y. Cao, L. Miao, S. Tanemura, M. Tanemura, Y. Kuno, and Y. Hayashi, Low resistivity p-ZnO films fabricated by sol-gel spin coating, Appl. Phys. Lett. **88**, 251116 (2006).

[23] S. Chou, M. Hon, and I. Leu, Synthesis of p-type Al-N codoped ZnO films using N_2O as a reactive gas by RF magnetron sputtering, Appl. Surf. Sci. **255**, 2958 (2008).

[24] K. Minegishi, Y. Koiwai, Y. Kikuchi, K. Yano, M. Kasuga, and A. Shimizu, Growth of p-type zinc oxide films by chemical vapor deposition, Jpn. J. Appl. Phys. **36**, L1453 (1997).

[25] D. Look, D. Reynolds, C. Litton, R. Jones, D. Eason, and G. Cantwell, Characterization of homoepitaxial p-type ZnO grown by molecular beam epitaxy, Appl. Phys. Lett. **81**, 1830 (2002).

[26] D. Snigurenko, K. Kopalko, T. Krajewski, R. Jakiela, and E. Guziewicz, Nitrogen doped p-type ZnO films and p-n homojunction, Semicond. Sci. Technol. **30**, 015001 (2015).

[27] W. Lambrecht and A. Boonchun, Identification of a N-related shallow acceptor and electron paramagnetic resonance center in ZnO:N_2^+ on the Zn site, Phys. Rev. B **87**, 195207 (2013).

[28] K. Tang, S. Zhu, Z. Xu, J. Ye, and S. Gu, Experimental investigation on nitrogen related complex acceptors in nitrogen-doped ZnO films, J. Alloys Comp. **696**, 590 (2017).

[29] C. Ton-That, L. Zhu, M. Lockrey, M. Philips, B. Cowie, A. Tadich, L. Thomsen, S. Khachadorian, S. Schlichting, N. Jankowski, and A. Hoffmann, Molecular nitrogen acceptors in ZnO nanowires induced by nitrogen plasma annealing, Phys. Rev. B **92**, 024103 (2015).

[30] Z. Wang, Y. Yue, and Y. Cao, Preparation and properties of nitrogen doped p-type zinc oxide films by reactive magnetron sputtering, Vacuum **101**, 313 (2014).

[31] S. Limpijumnong, X. Li, S.-H. Wei, and S. Zhang, Substitutional diatomic molecules NO, NC, CO, N_2 and O_2: Their vibrational frequencies and effects on p doping of ZnO, Appl. Phys. Lett. **86**, 211910 (2005).

[32] N. Nickel and M. Gluba, Defects in Compound Semiconductors Caused by Molecular Nitrogen, Phys. Rev. Lett. **103**, 145501 (2009).

[33] L. Liu, J. Xu, D. Wang, M. Jiang, S. Wang, B. Li, Z. Zhang, D. Zhao, C.-X. Shan, B. Yao, and D. Shen, p-Type Conductivity in N-Doped ZnO: The Role of the N_{Zn}-V_O Complex, Phys. Rev. Lett. **108**, 215501 (2012).

[34] J. Reynolds, C. Reynolds, Jr. A. Mohanta, J. Muth, J. Rowe, H. Everitt, and D. Aspnes, Shallow acceptor complexes in p-type ZnO, Appl. Phys. Lett. **102**, 152114 (2013).

[35] M. Amini, R. Saniz, D. Lamoen, and B. Partoens, The role of the V_{Zn}-N_O-H complex in the p-type conductivity in ZnO, Phys. Chem. Chem. Phys. **17**, 5485 (2015).

[36] J. Bang, Y.-Y. Sun, D. West, B. Meyer, and S. Zhang, Molecular doping of ZnO by ammonia: A possible shallow acceptor, J. Mat. Chem. C **3**, 339 (2015).

[37] D. Yong, H. He, Z. Tang, S.-H. Wei, and B. Pan, H-stabilized shallow acceptors in N-doped ZnO, Phys. Rev. B **92**, 235207 (2015).

[38] Z. Xu, K. Tang, S. Zhu, J. Ma, J. Ye, and S. Gu, Identification and tunning of zinc-site nitrogen-related complexes in ZnO material, J. Vac. Sci. Technol. A **36**, 021503 (2018).

[39] F. Tuomisto, C. Rauch, M. Wagner, A. Hoffmann, S. Eisermann, B. Meyer, L. Kilanski, M. Tarun, and M. McCluskey, Nitrogen and vacancy clusters in ZnO, J. Mat. Res. **28**, 1977 (2013).

[40] T. Borseth, F. Tuomisto, J. Christensen, E. Monakhov, B. Svenson, and A. Kuznetsov, Vacancy clustering and acceptor activation in nitrogen-implanted ZnO, Phys. Rev. B **77**, 045204 (2008).

[41] J. Villafuerte, E. Sarigiannidou, F. Donatini, J. Kioseoglou, O. Chaix-Pluchery, J. Pernot, and V. Consonni, Modulating the growth of chemically deposited ZnO nanowires and the formation of nitrogen- and hydrogen-related defects using pH adjustment, Nanoscale Adv. **4**, 1973 (2022).

[42] J. Villafuerte, O. Chaix-Pluchery, J. Kioseoglou, F. Donatini, E. Sarigiannidou, J. Pernot, and V. Consonni, Engineering nitrogen- and hydrogen-related defects in ZnO nanowires using thermal annealing, Phys. Rev. Mat. **5**, 056001 (2021).

[43] S. Pal, T. Rakshit, S. Singha, K. Asokan, S. Dutta, D. Jana, and A. Sarkar, Shallow acceptor state in ZnO realized by ion implantation and annealing route, J. Alloys Comp. **703**, 26 (2017).

[44] Z. Huang, H. Ruan, H. Zhang, D. Shi, W. Li, G. Qin, F. Wu, L. Fang, and C. Kong, Conversion mechanism of conductivity and properties of nitrogen implanted ZnO single crystals induced by post-annealing, J. Mat. Sci.:Mat. Electron. **30**, 4555 (2019).

[45] J. Stehr, S. Chen, W. Chen, L. Cai, S. Shen, and I. Buyanova, Identification of a nitrogen-related acceptor in ZnO nanowires, Nanoscale **11**, 10921 (2019).

[46] C. Lee, S. Park, J. Lim, and H. Kim, Growth of p-type ZnO thin films by using an atomic layer deposition technique and NH_3 as a doping source, Mat. Lett. **61**, 2495 (2007).

[47] M. Sarwar, B. S. Witkowski, A. Sulich, and E. Guziewicz, Low-temperature cathodoluminescence of nitrogen-doped ZnO films deposited at low-temperature by atomic layer deposition, Acta Phys. Pol. A **141**, 135 (2022).

[48] E. Guziewicz, E. Przezdziecka, D. Snigurenko, D. Jarosz, B. Witkowski, P. Dluzewski, and W. Paszkowicz, Abundant acceptor emission from nitrogen-doped ZnO films prepared by atomic layer deposition under oxygen-rich conditions, ACS Appl. Mat. Int. **9**, 26143 (2017).

[49] A. Krtschil, D. Look, Z.-Q. Fang, A. Dadgar, A. Diez, and A. Krost, Local p-type conductivity in n-GaN and n-ZnO layers due to inhomogeneous dopant incorporation, Phys. B **376-377**, 703 (2006).

[50] A. Krtschil, A. Dadgar, N. Oleynik, J. Blasing, A. Diez, and A. Krost, Local p-type conductivity in zinc oxide dual-doped with nitrogen and arsenic, Appl. Phys. Lett. **87**, 262105 (2005).

[51] K. Ando, T. Abe, T. Taya, Y. Ishihara, K. Endomoto, Y. Yamazaki, J. Yoshikawa, K. Fujino, H. Nakamura, T. Ohno, and H. Kasada, Structural instability of N-acceptors in homo- and heteroepitaxially grown ZnO by MBE, Phys. Stat. Sol. B **247**, 1453 (2010).

[52] F. Oba, A. Togo, I. Tanaka, J. Paier, and G. Kresse, Defect energetics in ZnO: A hybrid Hartree-Fock density functional study, Phys. Rev. B **77**, 245202 (2008).

[53] S. J. Clark, J. Robertson, S. Lany, and A. Zunger, Intrinsic defects in ZnO calculated by screened exchange and hybrid density functionals, Phys. Rev. B **81**, 115311 (2010).

[54] A. Adeagbo, G. Fisher, A. Ernst, and W. Hergert, Magnetic effects of defect pair formation in ZnO, J. Phys. Condens. Matter **22**, 436002 (2010).

[55] J. L. Lyons, J. B. Varley, D. Steiauf, A. Janotti, and C. G. V. de Walle, First-principles characterization of native-defect-related optical transitions in ZnO, J. Appl. Phys. **122**, 035704 (2017).

[56] Y. K. Frodason, K. M. Johansen, T. S. Bjørheim, B. G. Svensson, and A. Alkauskas, Zn vacancy as a polaronic hole trap in ZnO, Phys. Rev. B **95**, 094105 (2017).

[57] O. Volnianska, T. Zakrzewski, and P. Boguslawski, Point defects as a test ground for the local density approximation +U theory: Mn, Fe, and V_{Ga} in GaN, J. Chem. Phys. **141**, 114703 (2014).

[58] J. P. Perdew, R. G. Parr, M. Levy, and J. L. B. Jr., Density-Functional Theory for Fractional Particle Number: Derivative Discontinuities of the Energy, Phys. Rev. Lett. **49**, 1691 (1982).

[59] B. Himmetoglu, A. Floris, S. de Gironcoli, and M. Cococcioni, Hubbard-corrected DFT energy functionals: The LDA+U description of correlated systems, Int. J. Quantum Chem. **114**, 14 (2014).

[60] M. Cococcioni and S. de Gironcoli, Linear response approach to the calculation of the effective interaction parameters in the LDA+U method, Phys. Rev. B **71**, 035105 (2005).

[61] X. Ma, Y. Wu, Y. Lv, and Y. Zhu, Correlation effects on lattice relaxation and electronic structure of ZnO within the GGA+U formalism, J. Phys. Chem. C **117**, 26029 (2013).

[62] J. Villafuerte, F. Donatini, J. Kioseoglou, E. Sarigiannidou, O. Chaix-Pluchery, J. Pernot, and V. Consonni, Zinc vacancy–hydrogen complexes as major defects in ZnO nanowires grown by chemical bath deposition, J. Phys. Chem. C **124**, 16652 (2020).

[63] E. Guziewicz, M. Godlewski, L. Wachnicki, T. Krajewski, G. Luka, S. Gieraltowska, R. Jakiela, A. Stonert, W. Lisowski, M. Krawczyk, J. Sobczak, and A. Jablonski, ALD grown zinc oxide with controllable electrical properties, Semicond. Sci. Technol. **27**, 074011 (2012).

[64] K. Tang, R. Gu, S. Zhu, Z. Xu, Y. Shen, J. Ye, and S. Gu, Optical fingerprints of donors and acceptors in high-quality NH3-doped ZnO films, Opt. Mat. Express **7**, 1169 (2017).

[65] C. Lee and J. Lim, Dependence of the electrical properties of the ZnO thin films grown by atomic layer epitaxy on the reactant feed sequence, J. Vac. Sci. Technol. A **24**, 1031 (2006).

[66] P. Zeller, M. Amati, H. Sezen, M. Scardameglia, C. Struzzi, C. Bittencourt, G. Lantz, M. Hajlaoui, E. Papalazarou, M. Marino, M. Fanetti, S. Ambrosi, S. Rubini, and L. Gregoratti, Scanning photoelectron spectro-microscopy: A modern tool for the study of materials at the nanoscale, Phys. Stat. Sol. A **215**, 1800308 (2018).

[67] M. Amatti, A. Barinov, V. Feyer, L. Gregoratti, M. Al-Hada, A. Locatelli, T. Mentes, H. Sezen, C. Schneider, and M. Kiskinova, Photoelectron microscopy at Elletra: Recent advances and perspectives, J. Electron Spectr. Rel. Phenom. **224**, 59 (2018).

[68] J. P. Perdew, K. Burke, and M. Ernzerhof, Generalized Gradient Approximation Made Simple, Phys. Rev. Lett. **77**, 3865 (1996).

[69] P. Giannozzi, S. Baroni, N. Bonini, M. Calandra, R. Car, C. Cavazzoni, D. Ceresoli, G. L. Chiarotti, M. Cococcioni, I. Dabo, and A. Dal Corso, QUANTUM ESPRESSO: A modular and open-source software project for quantum simulations of materials, J. Phys.: Condens. Matter. **21**, 395502 (2009).

[70] D. Vanderbilt, Soft self-consistent pseudopotentials in a generalized eigenvalue formalism, Phys. Rev. B **41**, 7892 (R) (1990).

[71] H. J. Monkhorst and J. D. Pack, Special points for Brillouin-zone integrations, Phys. Rev. B **13**, 5188 (1976).

[72] See Supplemental Material at http://link.aps.org/supplemental/10.1103/PhysRevApplied.18.044021 for details of experimental measurements (Secs. S1–S3) and DFT calculations (Sec. S4.A-C). Supplemental Material includes the following sections: (S1) XRD patterns of ZnO and ZnO:N films, (S2) Scanning electron microscopy, (S3) SPEM results for the O1*s* level. (S4.B) The electronic structure of ZnO. (S4.C) The results of the DOS calculations for V_{Zn}, N_O, $V_{Zn}N_O$, $V_{Zn}N_OH$, and $V_{Zn}N_OH$-N_O, atomic configurations of the $V_{Zn}N_OH$-N_O and the spin-density distributions of $V_{Zn}N_OH$, N_O, and $V_{Zn}N_OH$-N_O are presented. References [99–102] are included in the Supplemental Material.

[73] S. B. Zhang and J. E. Northrup, Chemical Potential Dependence of Defect Formation Energies in GaAs: Application to Ga Self-Diffusion, Phys. Rev. Lett. **67**, 2339 (1991).

[74] S. Lany and A. Zunger, Accurate prediction of defect properties in density functional supercell calculations, Model. Simulat. Mater. Sci. Eng. **17**, 084002 (2009).

[75] D. D. Wagman, W. H. Evans, V. B. Parker, R. H. Schumm, I. Halow, S. M. Bailey, K. L. Churney, and R. L. Nuttall, The NBS tables of chemical thermodynamic properties. Selected values for inorganic and C1 and C2 organic substances in SI units, J. Phys. Chem. Ref. Data **11**, suppl 2 (1982).

[76] J. Lahiri, S. Senanayake, and M. Batzill, Soft x-ray photoemission of clean and sulfur-covered polar ZnO surfaces: A view of the stabilization of polar oxide surfaces, Phys. Rev. B **78**, 155414 (2008).

[77] M. Allen, D. Zemlyanov, G. Waterhouse, J. Metson, T. Veal, C. McConville, and S. Durbin, Polarity effects in the x-ray photoemission of ZnO and other wurtzite semiconductors, Appl. Phys. Lett. **98**, 101906 (2011).

[78] N. Ohashi, Y. Adachi, T. Ohsawa, K. Matsumoto, I. Sakaguchi, H. Haneda, S. Ueda, H. Yoshikawa, and K. Kobayashi, Polarity-dependent photoemission spectra of wurtzite-type zinc oxide, Appl. Phys. Lett. **94**, 122102 (2009).

[79] J. Williams, H. Yoshikawa, S. Ueda, Y. Yamashita, K. Kobayashi, Y. Adachi, H. Haneda, T. Ohgaki, H. Miyazaki, T. Ishigaki, and N. Ohashi, Polarity-dependent photoemission spectra of wurtzite-type zinc oxide, Appl. Phys. Lett. **100**, 051902 (2012).

[80] J. Chiou, J. Jan, H. Tsai, C. Bao, W. Pong, M. Tsai, I. Hong, R. Klauser, J. Lee, J. Wu, and S. Liu, Electronic structure of ZnO nanorods studied by angle-dependent x-ray absorption spectroscopy and scanning photoelectron microscopy, Appl. Phys. Lett. **84**, 3462 (2004).

[81] S. Ray, J. Chiou, W. Pong, and M.-H. Tsai, Electronic properties of nanomaterials elucidated by synchrotron radiation-based spectroscopy, Crit. Rev. Sol. State Mat. Sci. **31**, 91 (2006).

[82] S. Ansari, M. Khan, S. Kalathil, A. Nisar, J. Lee, and M. Cho, Oxygen vacancy induced band gap narrowing of ZnO nanostructures by an electrochemically active biofilm, Nanoscale **5**, 9238 (2013).

[83] D. Schmeißer, J. Haeberle, P. Barquinha, D. Gaspar, L. Pereira, R. Martins, and E. Fortunato, Electronic structure of amorphous ZnO films, Phys. Stat. Sol. C **11**, 1476 (2014).

[84] J. Wang, Z. Wang, B. Huang, Y. Ma, Y. Liu, X. Qin, X. Zhang, and Y. Dai, Oxygen vacancy induced band-gap narrowing and enhanced visible light photocatalytic activity of ZnO, ACS Appl. Mat. Int. **4**, 4024 (2012).

[85] S. Sakong, J. Gutjahr, and P. Kratzer, Comparison of density functionals for nitrogen impurities in ZnO, J. Chem. Phys. **138**, 234702 (2013).

[86] F. Gallino, G. Pacchioni, and C. D. Valentin, Transition levels of defect centers in ZnO by hybrid functionals and localized basis set approach, J. Chem. Phys. **133**, 144512 (2010).

[87] S. Lany and A. Zunger, Generalized Koopmans density functional calculations reveal the deep acceptor state of N_O in ZnO, Phys. Rev. B **81**, 205209 (2010).

[88] O. Volnianska, Magnetic properties of isolated Re ion and Re-Re complex in ZnO studied by GGA+U approach, J. Magn. Magn. Mater. **441**, 436 (2017).

[89] O. Volnianska and P. Boguslawski, Green luminescence and calculated optical properties of Cu ions in ZnO, J. Alloys Compd. **782**, 1024 (2019).

[90] M. Izaki and T. Omi, Transparent zinc oxide films prepared by electrochemical reaction, Appl. Phys. Lett. **68**, 2439 (1996).

[91] V. Srikant and D. R. Clarke, On the optical band gap of zinc oxide, J. Appl. Phys. **83**, 5447 (1998).

[92] O. Volnianska, P. Boguslawski, and E. Kaminska, Ag and N acceptors in ZnO: An ab initio study of acceptor pairing, doping efficiency, and the role of hydrogen, Phys. Rev. B **85**, 165212 (2012).

[93] S. J. Jokela and M. D. McCluskey, Unambiguous identification of nitrogen-hydrogen complexes in ZnO, Phys. Rev. B **76**, 193201 (2007).

[94] A. Janotti and C. G. V. de Walle, Native point defects in ZnO, Phys. Rev. B **76**, 165202 (2007).

[95] C. Freysoldt, B. Grabowski, T. Hickel, J. Neugebauer, G. Kresse, A. Janotti, and C. G. V. de Walle, First-principles calculations for point defects in solids, Rev. Mod. Phys. **86**, 253 (2014).

[96] C. G. V. de Walle and J. Neugebauer, First-principles calculations for defects and impurities: Applications to III-nitrides, J. Appl. Phys. **95**, 3851 (2004).

[97] L. Oikkonen, M. Ganchenkova, A. Seitsonen, and R. Nieminen, Formation, migration, and clustering of point defects in $CuInSe_2$ from first principles, J. Phys.: Condens. Matter **26**, 345501 (2014).

[98] J. Hu, H. Y. He, and B. C. Pan, Hydrogen diffusion behavior in N doped ZnO: First-principles study, J. Appl. Phys. **103**, 113706 (2008).

[99] F. Fabbri, M. Villani, A. Catellani, A. Calzolari, G. Cicero, D. Calestani, G. Calestani, A. Zappettini, B. Dierre, T. Sekiguchi, and G. Salviati, Zn vacancy induced green luminescence on non-polar surfaces in ZnO nanostructures, Sci. Rep. **4**, 5158 (2014).

[100] S. S. Parhizgar and J. Beheshtian, Effect of nitrogen doping on electronic and optical properties of ZnO sheet: DFT+U study, Comput. Condens. Matter **15**, 1 (2018).

[101] J. B. Varley, A. Janotti, C. Franchini, and C. G. V. de Walle, Role of self-trapping in luminescence and p-type conductivity of wide-band-gap oxides, Phys. Rev. B **85**, 081109(R) (2012).

[102] J. P. Allen and G. W. Watson, Occupation matrix control of d- and f-electron localisations using DFT + U, Phys. Chem. Chem. Phys. **16**, 21016 (2014).